

2 Size, Mass and Kinetics of Molecules

2.1 The Methods Determining the Size

2.1.1 Gas Laws and Density

The ideal gas law is hardly helpful in determining the size of molecules:

$$p V_m = R T \quad (2.01)$$

The volume V_m is the molar volume. For n moles, we have $V_m = V/n$. The gas constant has the value $R = 8,314510(70) \text{ J K}^{-1}\text{mol}^{-1}$. If we put into equ. (1) the pressure 0,1 MPa, the temperature 273,15 K and R , we get the molar volume of an ideal gas, which is considered a fundamental physical constant, and is $22,71108(19) \text{ L mol}^{-1}$ ($10^{-3}\text{m}^3 \text{ mol}^{-1}$). The values 0,1 MPa and 273,15 K should not be fused with the corresponding values for the standard condition in the physical chemistry:

- ➔ The standard condition convention of a substance in physical chemistry is the state of a pure substance at the normal pressure of 1 atm (101,33 kPa) and temperature of 25 °C (298,15 K), where gases should behave ideally.

If we divide the molar volume of an ideal gas by Avogadro's number ($N_A = 6,0221367 \times 10^{23} \text{ mol}^{-1}$), we get the volume occupied by a molecule, which is approximately $3,77 \times 10^{-26} \text{ m}^3$. The length of a side of this volume is about 3,35 nm for an ideal gas at 0 °C and 1 bar.

Now we use the volume of a mol of liquid water instead (about 18 cm^3), divide this by Avogadro's number and calculate the third root, we get a "diameter" of about 3,1 Å, which is more realistic. Here we use the unit Å parallel to the unit nm ($10 \text{ Å} = 1 \text{ nm}$).

Much more accurate results are obtained, if we calculate the molecular size from the covolume b in the real gas equation (a/V_m^2 is the internal pressure)

$$\left(p + \frac{a}{V_m^2} \right) (V_m - b) = R T \quad \text{with} \quad b = 4 N_A V_{\text{particle}} = 4 V_{\text{mole particles}}. \quad (2.02)$$

The right hand part of equ. (2.02) defines that for spherical molecules (atoms), the covolume b is equal to four times the internal volume of N_A particles.

By measuring the pV -diagram, and determining the parameter b by fitting the real gas equation, we get for water $b = 30,49 \times 10^{-6} \text{ m}^3 \text{ mol}^{-1}$ or $12,66 \times 10^{-30} \text{ m}^3$ per molecule. That gives us a diameter of 2,89 Å. Some further examples:

Molecule	Covolume $b/\text{L mol}^{-1}$	Covol.-diameter $d/\text{Å}$
H ₂	0,0266	2,76
O ₂	0,0318	2,93
CO ₂	0,0427	3,24
C ₆ H ₆	0,155	4,50

2.1.2 Transport Phenomena (Diffusion, Heat Conduction, Viscosity)

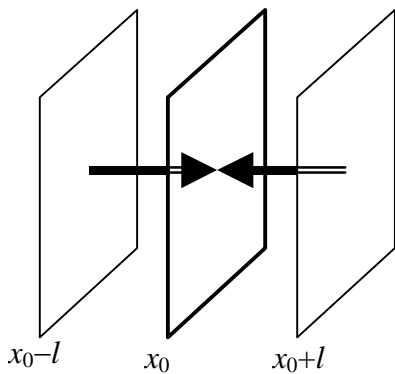
The three named phenomena can be mathematically described. We have:

$$\mathbf{j} = -C \text{ grad } \varphi \quad \text{and} \quad \dot{\varphi} = C \Delta \varphi, \tag{2.03}$$

(Do you know the meaning of the Nabla-operator (grad) ∇ and Laplace-operator Δ ?)

	Diffusion	Heat Conduction	Viscosity
\mathbf{j}	particle flow	heat flow	shearing stress
C	diffusion coefficient D	temperature conductivity $\lambda/c_v\rho$	viscosity η/ρ
φ	concentration n	temperature T	flow velocity

Equations (2.03) are Fick's first and second law of diffusion.



We can make statements about the mean free path using diffusion, heat conduction and viscosity:

Consider the flow of one type of molecule through a surface. This type of flow is due primarily to particles which are within one mean free path length l from both sides of the surface.

Molecules that reach the center surface per unit time (and per m^2) come from both the right and left side. That is

from the right side:
$$\frac{1}{6} n_{x_0+l} \langle v \rangle \approx \frac{1}{6} \left(n_{x_0} + l \frac{dn}{dx} \right) \langle v \rangle, \tag{2.04}$$

and from the left side:
$$\frac{1}{6} n_{x_0-l} \langle v \rangle \approx \frac{1}{6} \left(n_{x_0} - l \frac{dn}{dx} \right) \langle v \rangle, \tag{2.05}$$

where $\langle v \rangle$ is the mean of the absolute value of the velocity of the particles, which unlike the concentration should not depend on x . The difference of these two currents is

$$\frac{1}{3} l \langle v \rangle \frac{dn}{dx}. \tag{2.06}$$

A comparison of equ. (2.06) with equ. (2.03) (replace C with D and φ with n) gives

$$D = \langle v \rangle l / 3. \tag{2.07}$$

We can measure D , and $\langle v \rangle$ can be estimated with the aid of kinetic gas theory. Maxwell's distribution function for the mean square of the velocity is a function of the density ρ and pressure p :

$$\langle v \rangle^2 = \overline{v^2} = \frac{3p}{\rho}. \tag{2.08}$$

Similar considerations to mass transfer lead for the heat conductivity λ to

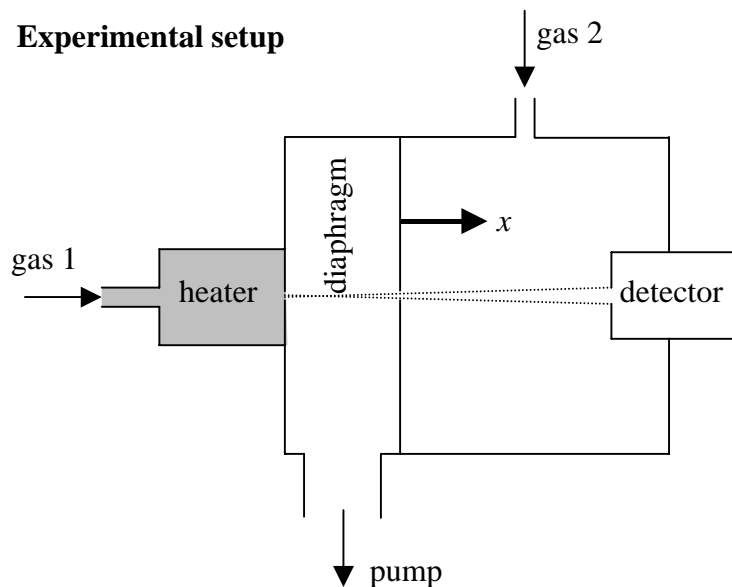
$$\lambda = \frac{1}{3} N \frac{C_V}{N_A} \sqrt{v^2} l, \quad (2.09)$$

where N is the number of molecules per m^3 , N_A is Avogadro's number, and C_V is the specific heat at constant volume. The inner viscosity η of the molecules is

$$\eta = l \sqrt{\frac{p\rho}{3}}. \quad (2.10)$$

We can thus make statements about the mean free path from the measured parameters of transport phenomena. If we set this length equal to the size of the molecule, we run into similar problems as with the use of the ideal gas law. We will derive a satisfactory correlation in the following chapter.

2.1.3 Scattering Cross Section



For the sake of simplicity, we will consider the identical particles (atoms or molecules) in the oven and scattering chamber, and assume that the concentration in the scattering chamber is so small, that no particles in the scattering direction are aligned. The probability W that a collision occurs is thus

$$W = \frac{\text{sum of all scattering cross sections in the flight path}}{\text{total area } A}$$

The scattering cross section σ in a collision of particle type 1 with type 2 would be $(r_1 + r_2)^2 \pi$, for identical particles it is $\sigma = 4r^2 \pi$. The sum of all scattering cross sections in the flight path is given by the product of the scattering cross section σ times the particle density per unit volume n time the surface area A time the length of the scattering chamber Δx .

If N particles pass the point x in the scattering chamber, WN particles are scattered out of the beam. We have

$$\Delta N = -\frac{\sigma n A \Delta x}{A} N. \quad (2.11)$$

Instead of a scattering chamber of length Δx let us consider many scattering chambers in series, each of the infinitesimal length dx , whose total length is L . From equ. (2.11), we get

$$\frac{dN}{N} = -n \sigma dx, \quad (2.12)$$

and integration leads us to

$$\ln N = -n \sigma x + \ln N_0, \quad (2.13)$$

where N_0 is the number of particles entering the chamber at $x = 0$. The measurement of the particle concentration at the detector gives:

$$N = N_0 e^{-n\sigma L}. \quad (2.14)$$

$n\sigma \equiv \alpha$ is called the macroscopic scattering coefficient and σ the microscopic total scattering cross section.

The direct determination of the scattering cross section in gases is often replaced by the measurement of the mean free path l , which we can define with equ. (2.14) as the path L , in which N has been reduced from N_0 to N_0/e . From equ. (2.14) we can also see that l is reciprocal of the macroscopic scattering coefficient:

$$l = \frac{1}{\sigma n} = \frac{1}{4\pi r^2 n} = \frac{1}{\pi d^2 n}. \quad (2.15)$$

Without proof we state that the consideration of the motion of the scattered molecules gives an extra factor of $\sqrt{2}$ in the denominator of equ. (2.15). Now we can determine l by the method mentioned in the previous chapter 2.1.2. We know the value n and obtain the size d of the molecule by means of equ. (2.15).

Gas kinetic diameters obtained from the mean free path l are given below and compared with the values obtained from the covolume, cf. chapter 2.1.1:

Molecule	Kinetic diameter $d/\text{\AA}$	Covol.-diameter $d/\text{\AA}$
H ₂	2,3	2,76
O ₂	3,0	2,93
CO ₂	3,4	3,24

2.1.4 X-ray, Electron, and Neutron Diffraction

The distances between atoms or molecules in solids can be measured using diffraction (interference) of radiation. Single crystals are preferable, but the methods also work with powdered samples of crystalline substances. The wave length of the diffracted light should be of the same order of magnitude as the distance between the atoms, about 1 Å. That is true for X-rays, slow neutrons (4 km s^{-1}) and electrons accelerated with 50 kV. Examinations of molecular crystals help us understand biological structures. In "X-ray amorphous" solids, for example glass, or in liquids the information we can obtain is limited to the short range order. *Structural* examinations using X-ray beams and slow neutrons have found a wide range of applications, but are not the subject of this chapter.

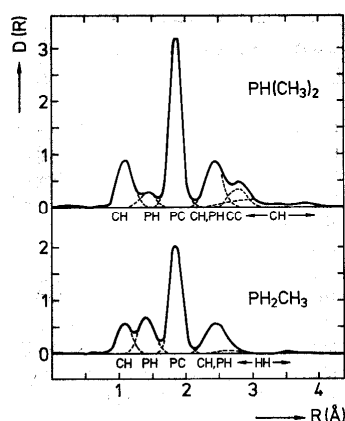


Abb. 2.1. Aus Elektronenbeugungs-Aufnahmen gewonnene radiale Verteilungsfunktion D der Elektronendichte als Funktion des Abstandes vom Kern R in den Molekülen $\text{PH}(\text{CH}_3)_2$ und PH_2CH_3 . Die Maxima in der Verteilungsfunktion können den angegebenen Kernkonfigurationen zugeordnet werden. (Nach Bartell, J., Chem. Phys. 32, 832 (1960))

The size of the molecules can be obtained from the distances between the atoms of a molecule by analyzing the distribution of the scattering intensities in the electron diffraction diagram, cf. figure on the left taken from Haken and Wolf. A complete structural analysis including the X-H-distances ($X = \text{C}, \text{N}, \text{O}, \text{P}, \text{etc.}$) can be obtained from the neutron diffraction. However, X-ray beams give the best structural analysis for the arrangement of the X-nuclei only.

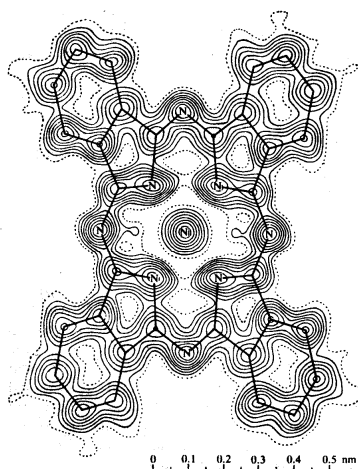


Abb. 2.9. Elektronendichte-Diagramm des Moleküls Nickel-Phthalocyanin. Ebenso wie in Abb. 2.2 sind die H-Atome nicht zu erkennen, weil sie durch Röntgen-Beugungs-Methoden neben Atomen mit größerer Elektronendichte schwer meßbar sind. Die Höhen-Konturlinien stellen die Elektronendichte dar. Sie verlaufen im Abstand von jeweils einem Elektron je Å^2 , wobei die gestrichelten Linien der Dichte von 1 Elektron je Å^2 entsprechen. Um das zentrale Ni-Atom herum beträgt der Linienabstand 5 Elektronen je Å^2 . Nach Robertson

X-ray also provides electron density maps by the evaluation of the reflex intensities with Fourier synthesis, cf. figure on the left taken from Haken and Wolf.

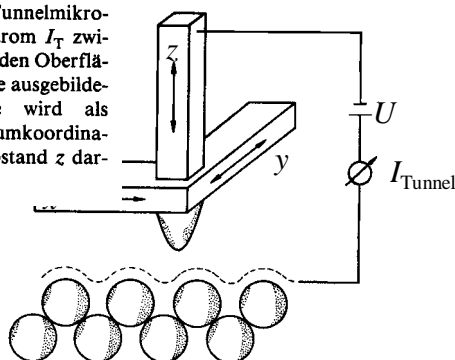
2.1.5 Microscopes

Since the wave length of the radiation limits the resolving power, optical microscopes can not resolve molecular structures. With transmission electron microscopes, resolutions of 1-2 Å have been reached as shown in some figures that were presented in Chapter 1.

Scanning electron microscopes focus an electron beam with electron optics at a small point on the surface of the sample and, by exciting the atoms there, create either emission of light or secondary electrons. The intensity of these emissions is measured as a function of two spatial coordinates.

Abb. 2.4. Schematische Darstellung eines Raster-Tunnelmikroskops. Der Tunnelstrom I_T zwischen der abzubildenden Oberfläche und der als Spitze ausgebildeten Gegenelektrode wird als Funktion der 3 Raumkoordinaten x, y und dem Abstand z dargestellt

point



In a scanning tunneling microscope, an extremely thin point is brought so close to a conducting surface, that under the operating voltage (mV to V), a current due to the tunnel effect can be measured. This current is kept at a constant value by controlling the distance between the tip and the surface. The image is created by recording the three dimensional coordinates of the point.

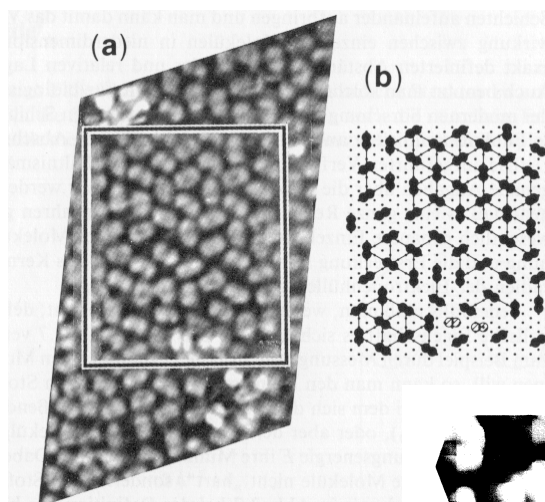
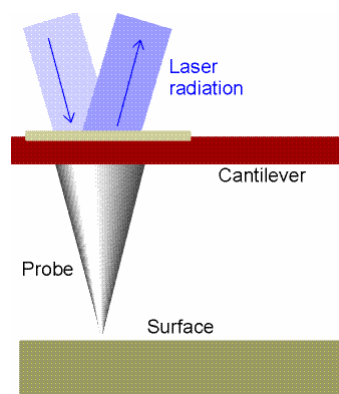


Abb. 2.5. (a) Rastertunnel-mikroskopische Abbildung von Naphthalin-Molekülen auf einer Pt (111)-Unterlage. (b) Schematische Darstellung der Orientierung der Naphthalin-Moleküle auf der Pt (111)-Unterlage. Aus V.M. Hallmark, S. Chiang, J.K. Brown, Ch. Wöll, Phys. Rev. Lett. **66**, 48 (1991). Für eine Übersicht sei verwiesen auf J. Frommer, Angew. Chem. **104**, 1325 (1992)

Figures 2.4, 2.5 and 1.5 were taken from Haken and Wolf.



Left: Fig. 28.22 taken from Atkins. A representation of the probe of an atomic force microscope. The probe tapers to a single atom; the deflection of the cantilever beam is monitored by using laser radiation reflected from a small mirror.

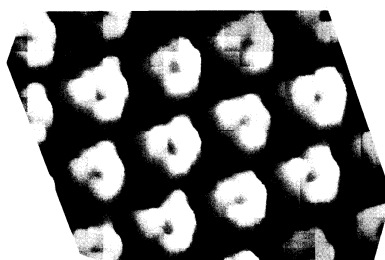


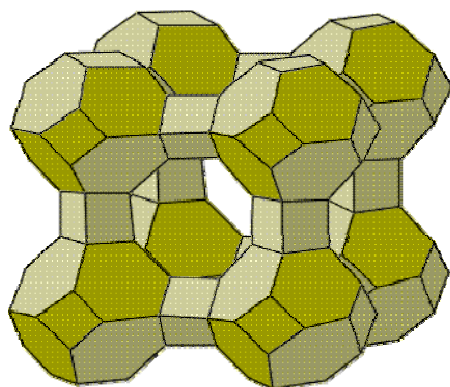
Abb. 1.5. Abbildung von Benzol-Molekülen mit dem Raster-Tunnel-Mikroskop. Die Benzol-Moleküle sind auf einer Rhenium (111)-Oberfläche aufgedampft, gemeinsam mit CO-Molekülen, die der Fixierung dienen und fast unsichtbar sind. Als Folge der Substrat-Molekül-Wechselwirkung erscheinen im Bild partiell lokalisierte Zustände, durch die sich die Benzolmoleküle mit reduzierter (dreizähliger) Symmetrie darstellen. Es werden also nicht die einzelnen C-Atome, sondern Molekülorbitale dargestellt. (Aus H. Ohtani, R.J. Wilson, S. Chiang, C.M. Mate, Phys. Rev. Lett. **60**, 2398 (1988) – Von R.J. Wilson zur Verfügung gestellt)

In an atomic force microscope (AFM), the force between the point and the sample is measured, as a function of location. The sample could be composed of molecules on a solid surface, though they do not have to be conductive as they must be in the scanning tunneling microscope. The position in the x - y plane is controlled, the deflection in the z -direction is measured by the deflection of a laser beam on a mirror that is fixed on the cantilever.

2.1.6 More about the Size and Shape of Molecules

Surfactant molecules form thin layers on the surface of a liquid solution. The films are called monolayers, if they are one molecule thick. It is called Langmuir-Blodgett film (Irving Langmuir and Katherin Blodgett) if the monolayer has been transferred to a solid support. The Langmuir-Blodgett layers are studied as a model for biomembranes and as a basis for molecular devices. Since the molecular weight is known, the number of molecules per unit area can be determined from the density of a layer, and that leads directly to the molecular size. Analogously, the measurement of the weight of molecules absorbed at the surface of a solid body (for example metal, graphite, or porous solid material) can give us the weight of a monolayer. From that we can determine the surface occupied by a molecule, if we know the total surface.

The size of a molecule can not, however, really be defined very well. Also electron density representations give us no exact molecular size, because the electron charge density does not give an exact border of the molecule, cf. figure on page 5. In determining the molecular volume with the covolume, an assumption that the molecule is spherical is made. Even the simple water molecule can neither be described by a sphere or a surface. The surface methods mentined above determine only the surface of the molecule.



If the size is in question, we need to know other parameters such as temperature and environment. For example, the number of water molecules that fit in a zeolite cavity (see figure on the left taken from Atkins) of a certain size depends strongly on the temperature and the interaction with the walls (ions).

Bonding distances (interatomic distances) and connecting angles, which strongly affect the size of molecules, can be measured more accurately than molecular size. This is done using X-ray, electron, and neutron diffraction and has a precision of $\pm 0,01 \text{ \AA}$ for the spacing, and $\pm 1^\circ$ for the angles.

H_2 : 0,74 \AA ; O_2 : 1,21 \AA ; CH: 1,12 \AA ; HF: 0,92 \AA ; HI: 1,61 \AA are some bonding distances of diatomic molecules. The evaluation of the known (covalent) bonding distances gives average bonding lengths. The following values of lengths in pm can be used for the estimation of covalent bonding distances:

H	37						
C	77	N	74	O	66	F	64
	67**		65**		57**		
	60***						
Si	118	P	110	S	104	Cl	99
					95**		
Ge	122	As	121	Se	104	Br	114
		Sb	141	Te	137	I	133

** and *** refer to multiple bonds. The length of a bond is the sum of two values.

2.2 Mass Spectrometry

We can get the molecular mass of an ideal gas by measuring the molar mass of 22,711 L at 273,15 K and 0,1 MPa, and dividing this value by Avogadro's number. By doing this, we average over a possible mixture of several isotopes, or a mixture of different chemical components. If we know the chemical composition and the amount of isotopes present, the determination of the molecular mass from the molar mass and the Avogadro number is a simple calculation.

Mass spectrometry is one of the most important tools, in order to get information about the chemical composition and abundance of isotopes. This technique is difficult to place in the methods of spectroscopy, because it separates ions based on different masses (divided by their charges) in static electric or magnetic fields and does not need the interaction with an electromagnetic field (except Fourier MS).

Mass spectrometry can be considered as a three-step-procedure:

- Creation of ions from neutral atoms or molecules, starting with a gas or solid body;
- Ion separation with respect to their mass using electric and magnetic fields;
- Electronic detection of the intensity of the separated ions.

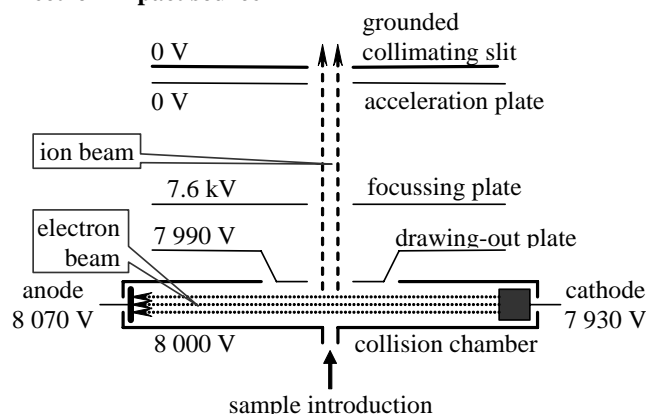
The mean free path has to be larger than the length of the instrument, in order to avoid collisions. Therefore, the mass separation is done in a high vacuum.

2.2.1 Ionization Techniques

The deflection in the static separation system does not only depend on the mass of the ion (or charge to mass ratio e/m with the elementary charge $e = 1,60217733(49) \times 10^{-19}$ C), but also on the speed of the ions. For this reason, all ions should have the same speed when they enter the deflection system. Speed-focusing deflection systems are applied in some deflection arrangements. Under consideration of quantitative statements, the relative rate of ion creation (singly ionized, less often doubly ionized, etc.) should be taken into account by calibrated response factors.

The selection of the ionization method depends on the one hand on the type of substance to be studied (vapor or solid), and on the other hand on the separation technique: single or double focusing static separation system, or a dynamic separation system. For the ionization of solid material, we can use thermal surface ionization, vacuum discharge, ion bombardment, electron bombardment, or photon bombardment.

Many substances can be vaporized if they are thermally stable. For the ionization of these substances, the electron impact source (electron bombardment, electron ionization) is used. The energy width of the ions is 0,1 to 1 eV.

Electron impact source

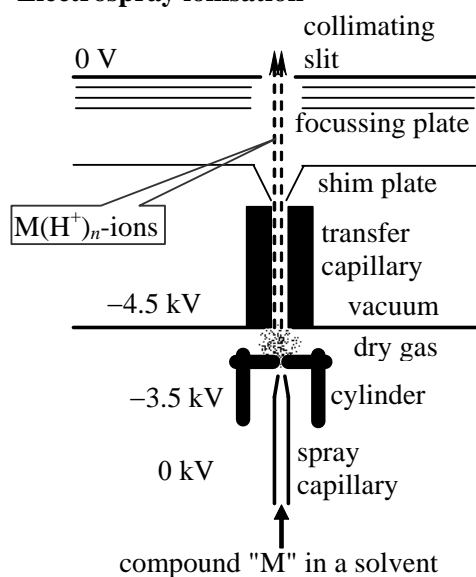
Ions are created, when the electron potential in the impact chamber (in the figure on the left the electron energy at the place of collision amounts about 70 eV) is equal to or larger than the ionization potential. The appearance potential in the mass spectrum is equal to (half) the minimum cathode-anode voltage at which the first ions appear.

For the ionization of a diatomic molecule AB, we have various possibilities. The most important primary and two secondary reactions are



A fragmentation of the molecule (ion) requires the input of the dissociation energy in addition to the ionization energy. From the appearance potential of the fragmentation, we can make statements about the dissociation energy of the separated bond.

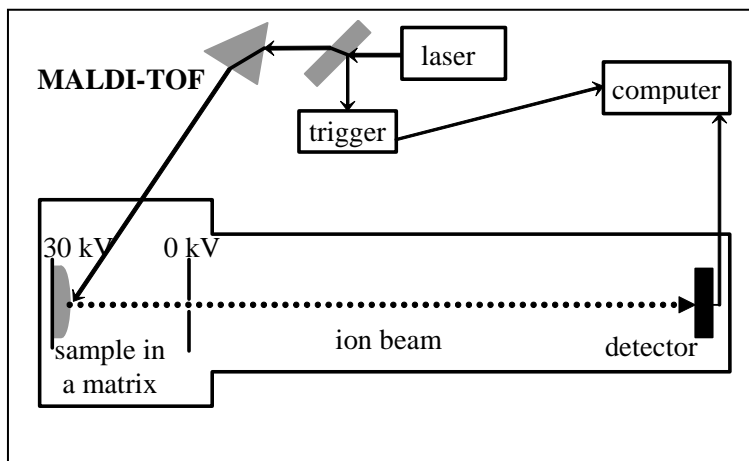
The chemical ionization, CI, is based on the electron impact source, which produces a primary ion. This reacts with a neutral molecule and creates (most commonly through proton transfer) a charged molecule. Fast atom bombardment, FAS, or ion bombardment are used to create secondary ions from solid body surfaces, where the solid body could be in a liquid or solid matrix.

Electrospray ionisation

Electrospray ionization, ESI, ionizes also thermally instable substances out of a liquid solution. It can be used to create positive or negative ions. Here we will describe the first case. The spray process begins when the force from a high voltage between the spray nozzle and the cylinder electrode on the ions in the liquid exceeds the force from the surface tension. At first, relatively large droplets with diameters of 1–10 μm are built. These strongly positively charged (H^+) droplets reduce their diameter due to two effects. First, a coulomb explosion occurs due to their strong positive charge. This process is finished, when sufficiently small particles (100 nm) are created whose attractive cohesive force is greater than the repulsive Coulomb force. Second, the liquid solvent evaporates in the atmosphere under the influence of a flowing dry gas. There remains a current of n -times

charged $\text{M}(\text{H}^+)_n$ ions, that enter the mass spectrometer after focusing. ESI is usually coupled in separation systems which are fed with slow ions.

The ion sources mentioned above work continuously and can therefore feed ions into the mass filter over a long period of time.



The matrix-assisted laser desorption/ionization, MALDI, works with laser pulses, and is preferred in time of flight (TOF) spectrometers.

The molecule under study is integrated in a rigid crystalline matrix with a mass ratio of about 1:1000. Laser pulses shorter than one nanosecond transfer energy onto the matrix, which absorbs laser light well and is supposed to

transfer protons onto the molecules. The obtained ions are accelerated with 30 kV. The speed v of singly charged ions of mass m is

$$eU = \frac{1}{2} m v^2, \quad (2.17)$$

where U is the accelerating voltage and e the absolute value of the elementary charge. Quadrupling the mass halves the speed, or doubles the time necessary to travel through the length of the apparatus (approx. 2 m or one free path length). Incoming particles are measured for about 1 ms with a resolution in the nanosecond range.

2.2.2 Static Separation Systems

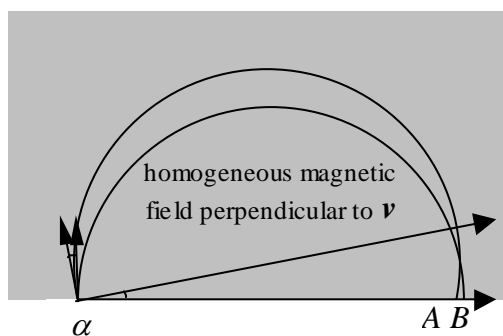
Electric and magnetic deflection systems act on ions in an analogous way to optical prisms or electron prisms: they produce dispersion, but also, under certain conditions, the focusing of a divergent beam in one direction. Lenses produce the same effect in two directions.

Deflection in a Magnetic Field

For a singly charged particle, in motion perpendicular to a homogenous magnetic field, we get

$$e \mathbf{v} \times \mathbf{B} \xrightarrow{\text{for } v \text{ perpendicular to } B} e v B = \frac{m v^2}{r} \Rightarrow \frac{1}{r} = \frac{e B}{m v} \quad (2.17a)$$

by setting the Lorentz force equal to the centrifugal force. After a complete revolution perpendicular to a homogenous magnetic field, we get a complete focusing of the divergence and the masses. A good focusing is also reached after 180° motion:



The appropriate orbital radius for the speed of the beam is r . From that we get a distance $\overline{AB} = 2r(1 - \cos \alpha) \approx \alpha^2 r$ when $\alpha \ll 1$. If the beam had not traveled in a circular orbit, the length of divergence after traveling the same distance would have been $r\pi\alpha$.

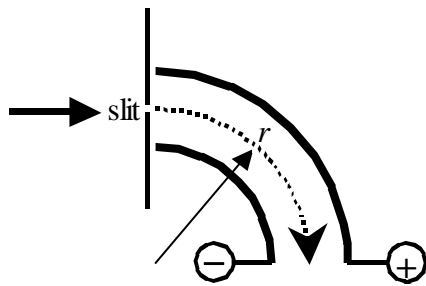
Deflection in an Electric Field

Let us now consider positive ions of mass m , created, for example, in an electron impact ion source. These ions are then accelerated through a potential difference U_B to the speed v_x in the x -direction ($eU_B = mv_x^2/2$). This speed stays constant during deflection in a parallel-plate capacitor, if the plates are lined up perpendicular to the y -direction. The distance between the plates is d and the capacitor voltage U_K . The capacitor voltage produces a electric field E and therefore an acceleration in the y -direction with $m\ddot{y} = eE = eU_K/d$. We have

$$\frac{eE}{m} = \ddot{y} = \frac{d}{dt} \frac{dy}{dt} = \frac{d}{dx} \frac{dx}{dt} \frac{dy}{dx} \frac{dx}{dt} = v_x^2 \frac{d^2 y}{dx^2}. \quad (2.18)$$

By integration, with the constants of integration $y_0 = v_{y0} = 0$, we get the parabolic path

$$y = x^2 \frac{eE}{2mv_x^2} = x^2 \frac{U_K}{4dU_B}. \quad (2.19)$$

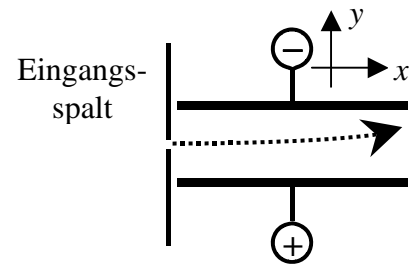


If we consider a cylindrical capacitor, with an average radius r , in place of a parallel-plate capacitor, the radial acceleration of a particle moving at constant speed in a circular path in the middle between the two cylindrical plates must be compensated by the acceleration by the electric field. We have:

$$\frac{mv^2}{r} = eE \Rightarrow \frac{1}{r} = \frac{e}{m} \frac{E}{v^2} = \frac{U_K}{2dU_B}. \quad (2.20)$$

The electric field in a parallel-plate capacitor and cylindrical capacitor achieves a focusing of divergent beam bundles similar to that of a magnetic field. In a cylindrical capacitor, the radius of a stable circular path increases with v^2 , but in a magnetic field, the orbital radius increases linearly with the speed. With that, we can achieve a focusing of speeds by combining both deflection systems.

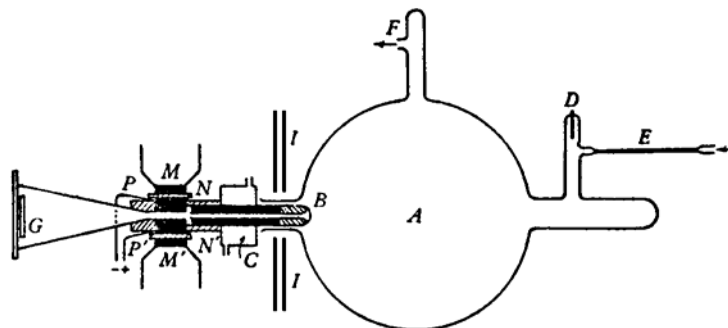
Since the ion bundles entering the separation system are both divergent and contain ions of differing speeds, we have two focusing problems. As in photography and other spectroscopic methods, we can trade off sharpness (resolution) for light-gathering power (detection sensitivity). By combining deflection systems, we have, however, a better way of solving the problem.



Thomson's Parabola Apparatus (Joseph John Thomson 1912: existence of both neon isotopes 20 and 22, first proof of isotopes) uses an almost parallel bundle of positive rays, which run between two poles of a magnet, upon which are mounted capacitor plates. The ions are deflected proportional to e/m in parallel electric and magnetic fields, proportional to $1/v^2$ in the direction of the field, and proportional to $1/v$ perpendicular to it. There is no focusing, different speeds produce different parabolas.

Fig. 1.1 taken from Duckworth et al.:

Thomson's positive-ray parabola apparatus. The letters indicate the following: *A*, discharge tube; *B*, cathode; *C*, water jacket for cooling cathode; *D*, anode; *E*, gas inlet; *F*, pump lead; *G*, photographic plate; *I*, magnetic shield; *M*, *M'*, magnetic poles; *N*, *N'*, mica for electrical insulation of *P*, *P'*, which are pieces of soft iron to serve both as condenser plates and to define the magnetic field. (From Aston, 1942.)



The Dempster Mass Spectrometer (1918) uses the directional focusing properties of a 180° magnetic fields. Arthur Jeffrey Dempster used it from 1920-22 to determine the abundance ratio of isotopes in N, Li, K, Ca and Zn.

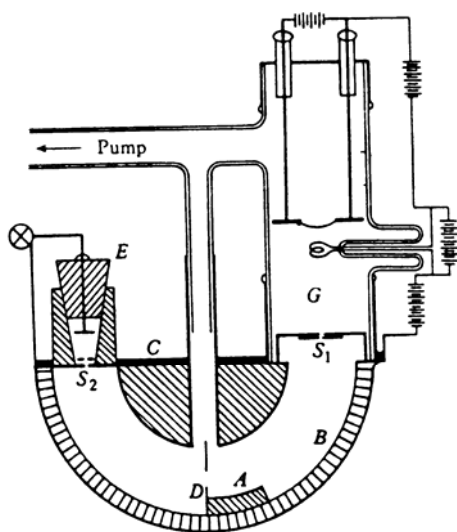


Fig. 1.3 taken from Duckworth et al.: Dempster's first mass spectrograph. *A* indicates the analyzing chamber, *B* and *C* are brass walls of the vacuum chamber, *D* is a diaphragm to prevent transmission of reflected rays, *E* is the ion collector unit, *G* is the ion source region, *S*₁ and *S*₂ are slits. (From Dempster, 1918.)

The Aston mass spectrometer, first version by Francis William Aston 1919, final proof of the two neon isotopes and the approximately whole number masses of other isotopes, Cl, Hg, N, Noble gases, but in 1923 the first observation of the divergence from whole number isotope masses. A parallel ion bundle is collimated and a focusing of speeds is reached with $E \perp H$.

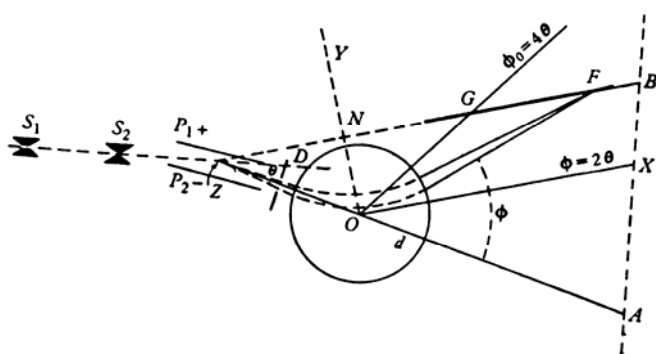
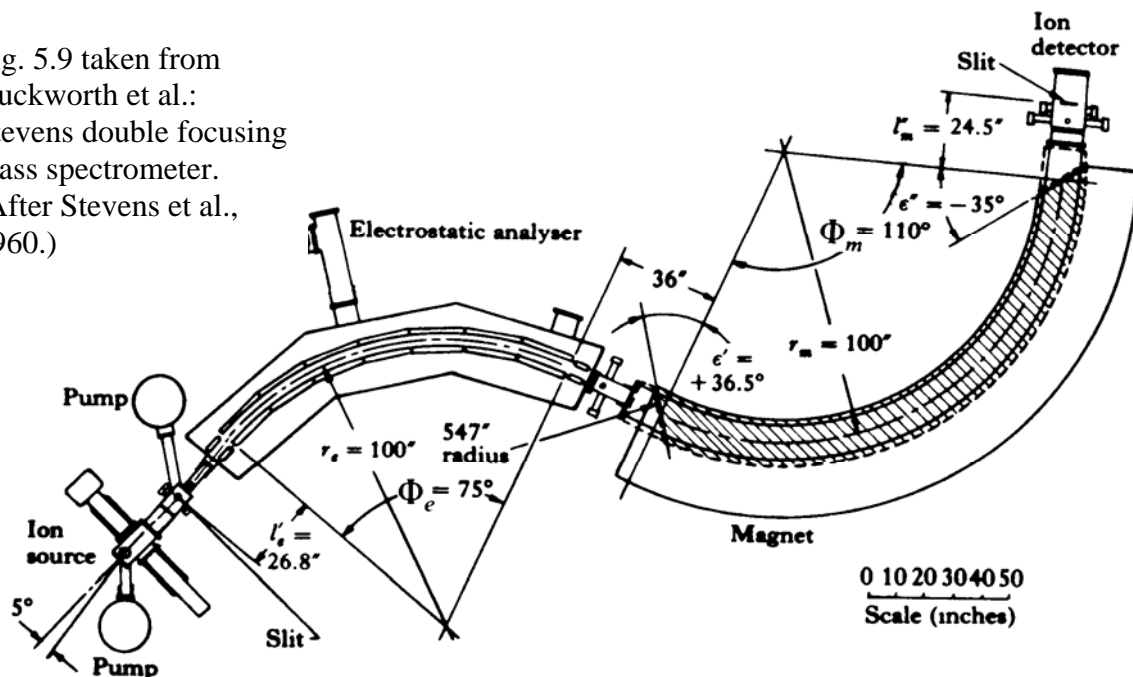


Fig. 1.2 taken from Duckworth et al.: The scheme of Aston's mass spectrograph. *S*₁ and *S*₂ are collimating slits, *P*₁ and *P*₂ are condenser plates, *D* is a diaphragm for selecting a portion of the beam emerging from the condenser, *Z* is the virtual source for the rays emerging from the condenser, *O* is the center of the uniform magnetic field, *GF* is the photographic plate, θ and ϕ are the deflections in the electric and magnetic fields, respectively. (From Aston, 1942.)

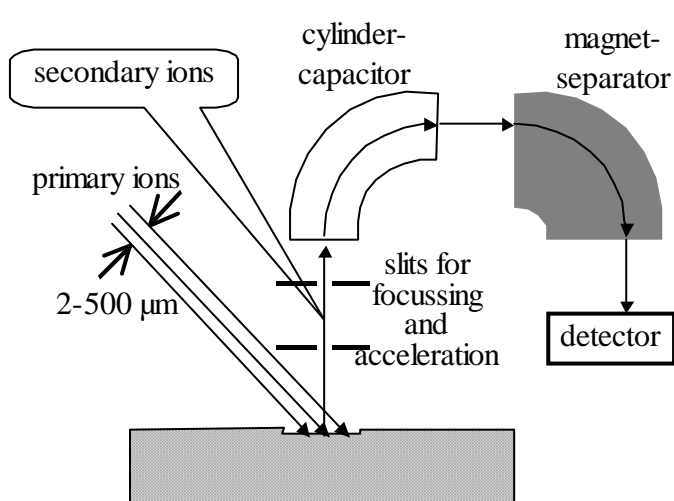
Single focusing mass spectrometers achieve either a speed or direction compensation with a capacitor and/or magnet. Double focusing mass spectrometers by Herzog, Mattauch, and other, achieve a speed and directional focusing with a capacitor and magnet.

Fig. 5.9 taken from Duckworth et al.: Stevens double focusing mass spectrometer. (After Stevens et al., 1960.)



The resolution is given as $m/\Delta m$, where Δm denotes the mass difference and m the mass average of two masses, which can just be resolved. The value (for single-charged ions) is about 10 for the Thomson parabola apparatus, 130 for the first Aston mass spectrometer, about 1000 for a single focusing device, between 1000 and 30 000 for TOF, 100 000 for double focusing devices, and reaches for Fourier spectrometers 1 000 000 in the case of small molecules (only 10 000 for a mass unit of 600).

2.2.3 Spatially Resolving Method SIMS



In the secondary ion mass spectrometry (SIMS), the solid body surface is struck with energetic ions, and the emitted ions are analyzed with a mass spectrometer. The primary beam (O_2^+ , O^- , Ar^+ or Cs^+) can be focused and aimed at the sample. A beam diameter of minimum 2 μm makes possible the micro analysis of the surface. The erosion of the surface layer by the primary ion beam gives a depth profile.

2.2.4 Dynamic Separation Systems

Static separation systems were dominantly used in the past. They still find applications for the exact determination of the isotopic ratio (IMRS, *isotop ratio mass spectrometry*). Modern mass spectrometry in organic chemistry and biology is based on a time dependent ion inlet and/or a time dependent electric or electromagnetic field. Corresponding spectrometers are often divided into time of flight and rf-spectrometers with or without a static magnetic field. The time of flight spectrometer without a magnetic field (TOF) has already been discussed in chapter 10.1.

Quadrupole mass filters are very cheap and fast scanning. Therefore they are often used in mass spectroscopy and in connection with other separation techniques like chromatography. Four bars (or one bar with two planes of reflection as a monopole filter) allow the creation of an electric potential with a quadratic dependency on the coordinates x and y (the bars point along the z -axis) with the following form:

$$U = U_0 \frac{x^2 - y^2}{2r_0^2}. \quad (2.21)$$

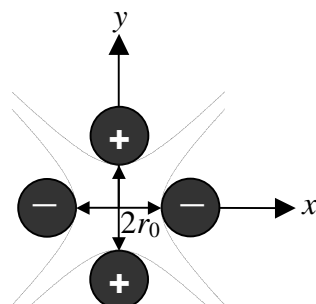


Figure on the left: Geometry of a quadrupole mass filter. The z -direction is perpendicular to the plane of the drawing. The electrodes are at the potentials $\pm U_0/2$, i.e. between neighboring electrodes there is a potential difference of U_0 . The distance between opposing electrodes is $2r_0$. The dotted lines show what the outer contours of the electrodes would be like if hyperbolic instead of circular electrodes had been used.

The quadrupole mass spectrometer was developed in 1953 from Wolfgang Paul and Helmut Steinwedel. Since it captures ions in a path on the z -axis, it is also referred to as Paul's ion trap. In these ion traps, single ions can be captured, if the a mass separation is performed first (so-called MS-MS coupling). In a quadrupole mass spectrometer, an ion current is injected along the z -direction ($x_0 = y_0 = 0$). A high frequency (rf) potential is added to the DC (static) voltage:

$$U_0 = U_{\text{static}} + U_{\text{rf}} \cos \omega t. \quad (2.22)$$

The superposition of U_0 and $-U_0$ at positive and negative electrodes, respectively, creates a hyperbolic field symmetric with respect to the z -direction (this is not axial symmetry; the z axis is a four fold symmetry axis for a rotary reflection). The equation of motion is described by the Mathieu differential equation. They apply to x (and y after changing the sign of the parenthesis in equ. (2.23)) and are exactly solvable for hyperbolically formed electrodes, and in approximately also solvable for electrodes with a circular cross section near $x = y = 0$.

$$\frac{d^2 x}{d\tau^2} + (a + 2b \cos 2\tau)x = 0 \quad \text{mit} \quad a = \frac{4eU_{\text{statisch}}}{m\omega^2 r_0^2}; \quad b = \frac{2eU_{\text{HF}}}{m\omega^2 r_0^2}; \quad \tau = \frac{\omega t}{2}. \quad (2.23)$$

Equation (2.23) indicates, that $a/2$ is the relationship between the potential energy in a static field to the kinetic energy of the vibration with a radius r_0 , and b is the relationship between the potential energy in the rf-field to the kinetic energy. A precise understanding of the processes necessitates a careful consideration of the solutions of these equations.

When U_{static} , the solutions give us the condition that $b < 0,46$ for a stable trajectory of the vibrating ion. This tells us that the kinetic energy of the vibration has to be larger than the potential energy in the rf-field, see equ. (2.23). If we additionally apply the static potential $U_{\text{static}} \neq 0$, the conditions for a stable trajectory are stronger limited. For example, if $U_{\text{static}}/U_{\text{rf}} = 0,166$, only masses with

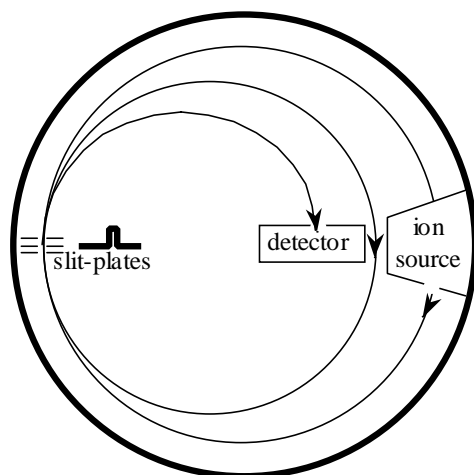
$$\frac{1}{b} = \frac{m r_0^2 \omega^2}{e 2U_{\text{HF}}} = 2,83 \quad (2.24)$$

can pass the filter. Equation (10.10) is given here without proof. Other ions are deflected and hit the electrodes (length approx. 10–50 cm).

The next described mass synchronometer and the Omegatron have little importance for the up-to-date mass spectrometry. But the revolution of ions in the magnetic field in the mass synchronometer and the ion cyclotron resonance in the omegatron are basics of the modern Fourier-transform mass spectroscopy.

Mass synchronometers are time of flight spectrometers with magnetic fields. After a complete revolution in the magnetic field, there is a perfect double focusing in the plane perpendicular to the magnetic field for all directions, speeds, and masses. The time of revolution t or the angular frequency ω are used as a new principle of separation.

$$t = \frac{2\pi r}{v} \quad \text{and} \quad r = \frac{mv}{eB} \Rightarrow t = \frac{2\pi m}{eB} \Rightarrow \omega = \frac{eB}{m} \quad (2.25)$$

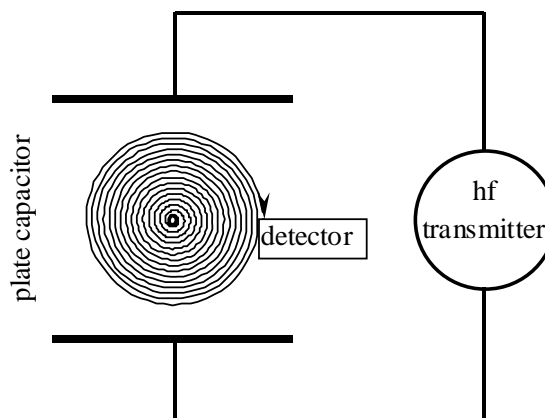


The ion inlet is performed continuously from the ionization chamber. The exiting ion beam strikes the back wall and is lost. With the help of a square wave pulse on the slit-decelerator, ion bundles are created from the continuous beam that travels several times around a path with a smaller diameter. A query pulse is sent which forces the ions traveling through the slits when the pulse is present onto still smaller circular orbits which lead to the detector.

Figure on the left: The mass synchronometer in a homogenous magnetic field perpendicular to the plane of the drawing. Decelerating pulses are applied to the slit plates.

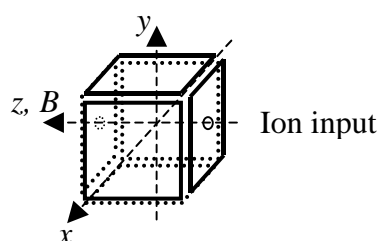
Figure on the right: The Omegatron.

The field lines of the homogenous magnetic field run perpendicular to the plane of the diagram. The electric field lines lie in the plane of the drawing, between the plates of the capacitor. The path from the cathode to the anode is perpendicular to the plane of the drawing in the middle of the capacitor. The ions in resonance move along spiral paths in the plane of the drawing until they hit the detector.



The Omegatron is a high frequency spectrometer with a magnetic field. The path between the cathode and anode for the electron impact ionization is parallel to the magnetic field and perpendicular to the electric field. The angular frequency of the ions is the same as in a mass synchronometer ($\omega = Be/m$). The rf is linearly polarized, and can be separated into two circular polarized fields. In a slow sweep of the magnetic field or the frequency, a signal is picked up in the target if resonance conditions are fulfilled, since in that case ions gain kinetic energy, and v and r are increased.

Fourier mass spectrometers use ion cyclotron resonance (ICR) like an Omegatron. A cryo-magnet (4–20 T) with a sufficient room temperature gap is necessary. The difference between the Fourier mass spectrometer and an Omegatron lies in the detection: there is no target, but



rather two “transmitter” plates oriented perpendicular to the x -direction and two “receiver” plates oriented perpendicular to the y -direction, which receive signals from the ions following circular orbits perpendicular to the magnetic field. The ions are introduced along the z -direction. There is only a direct voltage applied to the plates perpendicular to the z -direction. The frequencies correspond to the cyclotron resonance $Be m^{-1}$, i.e. for a

relative mass M_r (multiples of the unit u or Dalton) of a singly charged ion, and $B = 10$ T follows $\nu/\text{MHz} = 153,567 / M_r$.

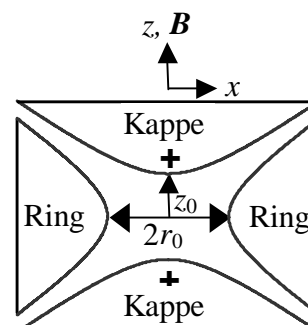
The Fourier experiment (FT-ICR or FT-MS) uses a short (ms range) powerful rf-pulse. The signal is observed with phase sensitive detection in the time scale after the ring down of the rf-pulse. A Fourier-transformation is used to obtain the mass spectrum. A large mass range from 10–4000 u ($1 u \equiv m_u = m_a(^{12}\text{C})/12 = \text{unified atomic mass unit} = 1 \text{ dalton} = 1 \text{ Da} \approx 1,66054 \times 10^{-27} \text{ kg}$) and extremely high resolutions are possible, approx. 300 000 for 150 u and several million for small masses.

Ion cyclotron resonance spectrometer in connection with a Penning trap reach resolutions of 10^8 , the highest today. A Penning trap is composed of a axially symmetric setup of hyperbolic cathodes, overlapped with a homogenous magnetic field along the axis of symmetry. The difference to quadrupole filters lies in the axial symmetry and the different distances from the rings and caps to the midpoint. The trap keeps the ions in stable trajectories, even in the z -direction, as long as they do not absorb energy from the rf-pulses.

Figure at right: The Penning trap. The homogenous magnetic field lies along the z -direction, the static electric field is applied to both caps. The induced signal voltage is measured between the caps on the grounded rings.

The homogenous magnetic field B creates stable circular orbits in the x - y -plane. To stabilize the z -direction of the positively charged ions, a voltage U_0 is applied to both caps, while the ring is grounded. Thereby we get an axially symmetric potential around the z -direction

$$U(r, z) = U_0 \frac{r^2 - z^2}{2r_0^2}. \quad (2.26)$$



The magnetic field causes a circular motion of the ions in an x - y -plane with the cyclotron frequency $\omega_{\text{cyclotron}} = eB/m$. Overlapped on this is an oscillation with the frequency ω_{electric} in the z -direction caused by the static electric field (returning force for displacement of the ions in the z - or $-z$ -direction). A third slow rotation in the x - y -plane happens like in a magnetron. The magnetron is a microwave generator with a ring shaped delay line, in which a radial electric field crosses an axial magnetic field creating the angular frequency $\omega_{\text{magnetron}} = E/Br$.

The magnetron frequency of the Penning trap is composed of a doublet with the frequencies

$$\omega_{\pm} = \frac{\omega_{\text{magnetron}}}{2} \pm \sqrt{\frac{\omega_{\text{cyclotron}}^2}{4} - \frac{\omega_{\text{electric}}^2}{2}}. \quad (2.27)$$

The frequency analysis of the induced signals gives very sharp line profiles (<1 Hz) for the cyclotron frequency, which is in the MHz range.

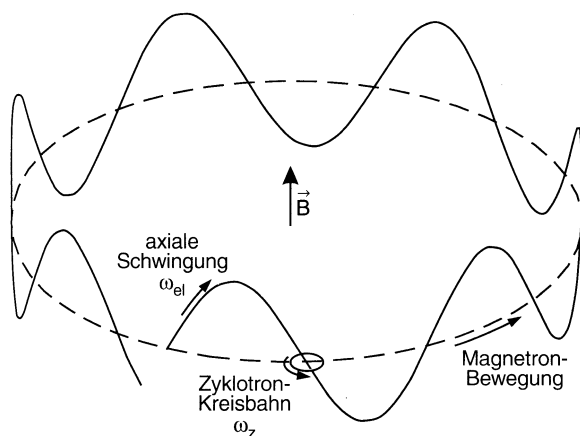


Fig. 2.74 taken from Demtröder. Decomposition of the orbital motion of an ion in cyclotron motion, the axial oscillation and the drift of the center of the circle in the direction of the field

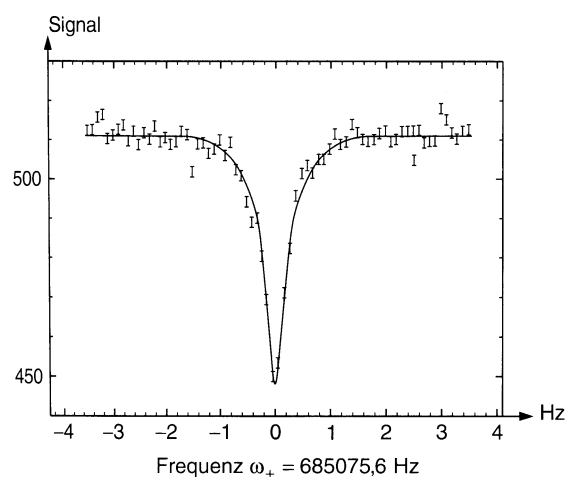


Fig. 2.75 taken from Demtröder. Example of the mass resolution of the cyclotron mass filter. Shown is the width of the resonance frequency ω_+ for the $^{133}\text{Cs}^+$ ion.

2.2.5 Mass Spectrometer Coupling

To increase the mass resolution, the mass spectrometer is sometimes preceded by a chromatographic separating column or another mass spectrometer. The later setup is called a tandem mass spectrometer, the process referred to as MS-MS-coupling. The most common is the coupling with a gas chromatograph (gas chromatography mass spectrometry, GC-MS) and with liquid chromatographs (liquid chromatography-mass spectrometry, LC-MS). Using a Fourier mass spectrometer with a Penning trap, we can use the $(\text{MS})^n$ process by repeating ion separation by application of rf-pulses and storing in trap. ((Chromatography should be shortly described here.))

2.2.6 Applications

The main application is the determination of ion masses or fragment masses in atomic mass units m_a , their proportional frequency and their appearance potential. High resolution allows the differentiation between different molecules and fragment ions with similar m_a .

The atomic masses m_a are expressed in multiples of the atomic mass unit m_u :
 $m_u = m_a(^{12}\text{C})/12 = 1 \text{ u} = 1 \text{ dalton} = 1 \text{ Da} = 1,6605402(10) \times 10^{-27} \text{ kg}$.

The most frequent area of application is the analytic organic chemistry, but also ever more in biochemistry. Many other applications cover a wide field:

- Ionization and dissociation of inorganic molecules,
- Examination of non-covalent ionic-molecular interactions;
- Determination of the abundance of isotopes in nature and in atomic reactions;
- Determination of the atomic masses of stable and radioactive isotopes;
- Examination of surfaces and modification of surfaces, ion implantation;
- Geology and Cosmology, especially age determination;
- Examination of the upper atmosphere and space research.

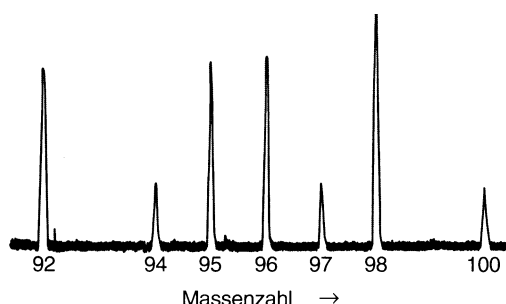


Fig. 2.76 taken from Demtröder. Abundance of isotopes in molybdenum, measured with double focusing mass spectrometer of *Mattauch*

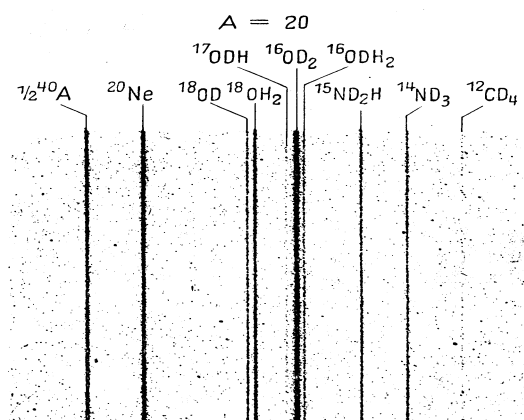


Fig. 19 taken from Finkelburg. Fine structure mass spectrogram by Bieri, Everling and *Mattauch* to demonstrate outstanding resolution of tiny mass differences (Separation of 10 different Ions of mass number 20, whose atomic or molecular weight range from 19,9878 to 20,0628).

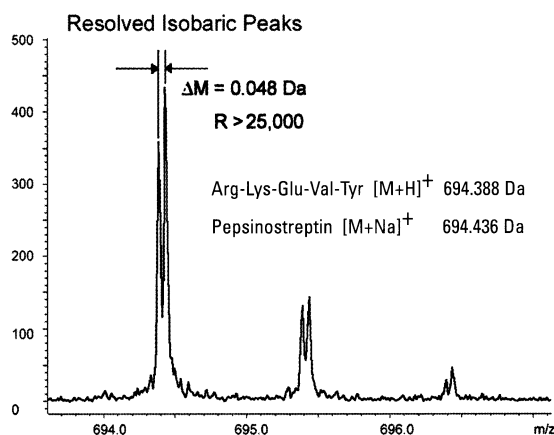


Figure on the left: Taken from Bruker Daltronics 2001, BioTOF II with COMPASS (coaxial multipass)

2.3 Specific Heat and Kinetic Energy

From mechanics we know that the average kinetic energy of molecules of mass m in gases is a function of the average value of the square of the velocities, as long as we ignore the rotation and vibration energy:

$$\overline{E}_{\text{kin}} = \frac{m}{2} \overline{v^2}. \quad (2.28)$$

For the pressure p of N particles per m^3 , with the help of thermodynamics, we get

$$p = \frac{2}{3} N \overline{E}_{\text{kin}}. \quad (2.29)$$

From the ideal gas law, see equ. (2.01), it follows for 1 mol and for a single molecule

$$\overline{E}_{\text{kin}} = \frac{3}{2} RT \quad \text{and} \quad \overline{E}_{\text{kin}} = \frac{3}{2} kT \quad (2.30)$$

respectively. The Boltzmann constant is $R/N_A = k = 1,380658(12) \times 10^{-23} \text{ J K}^{-1}$. Equation (2.28) only takes into consideration the translational motion with 3 degrees of freedom, which is correct for atoms. The specific heat at a constant volume is, according to definition (E stands for the inner energy, which is otherwise referred to as U)

$$C_V = \left(\frac{\partial E}{\partial T} \right)_V = \frac{3}{2} R. \quad (2.31)$$

For the specific heat at constant pressure, which we get by definition with the enthalpy $H = U + pV$ and the ideal gas law (1) $p V_m = R T$

$$C_p = \left(\frac{\partial H}{\partial T} \right)_p = C_V + R = \frac{5}{2} R. \quad (2.32)$$

These values are measure in atomic gases, but are too low in molecules due to the incorrect assumptions made in equation (2.28): the neglecting of the rotational and vibrational energy. It is east to see in the temperature dependent heat capacity $C_V(T)$ of the hydrogen molecule that at low temperatures, only the translational degrees of freedom are excited. At higher temperatures, the two degrees of freedom of rotation begin to play a role, and at very high temperatures, vibrations begin, see Fig. 2.12 taken from Haken and Wolf for the H_2 -molecule on the right. Every vibration has two degrees of freedom, one being the kinetic and the other being the potential energy.

